Geophysical Journal International

Geophys. J. Int. (2010) **182,** 1267–1278 doi: 10.1111/j.1365-246X.2010.04706.x

Joint full-waveform analysis of off-ground zero-offset ground penetrating radar and electromagnetic induction synthetic data for estimating soil electrical properties

D. Moghadas,[1] F. André,[1] E. C. Slob,[2] H. Vereecken[1] and S. Lambot[1,3]

[1]*Agrosphere* (ICG-4)*, Institute of Chemistry and Dynamics of the Geosphere, Forschungszentrum Jülich GmbH* 52425 *Jülich, Germany. E-mail: d.moghadas@fz-juelich.de*

[2]*Department of Geotechnology, Delft University of Technology, Stevinweg* 1, 2628 *CN Delft, the Netherlands*

[3]*Earth and Life Institute, Université catholique de Louvain, Croix du Sud* 2 *Box* 2, B-1348 *Louvain-la-Neuve, Belgium*

Accepted 2010 June 16. Received 2010 June 14; in original form 2010 January 7

SUMMARY

A joint analysis of full-waveform information content in ground penetrating radar (GPR) and electromagnetic induction (EMI) synthetic data was investigated to reconstruct the electrical properties of multilayered media. The GPR and EMI systems operate in zero-offset, off-ground mode and are designed using vector network analyser technology. The inverse problem is formulated in the least-squares sense. We compared four approaches for GPR and EMI data fusion. The two first techniques consisted of defining a single objective function, applying different weighting methods. As a first approach, we weighted the EMI and GPR data using the inverse of the data variance. The ideal point method was also employed as a second weighting scenario. The third approach is the naive Bayesian method and the fourth technique corresponds to GPR–EMI and EMI–GPR sequential inversions. Synthetic GPR and EMI data were generated for the particular case of a two-layered medium. Analysis of the objective function response surfaces from the two first approaches demonstrated the benefit of combining the two sources of information. However, due to the variations of the GPR and EMI model sensitivities with respect to the medium electrical properties, the formulation of an optimal objective function based on the weighting methods is not straightforward. While the Bayesian method relies on assumptions with respect to the statistical distribution of the parameters, it may constitute a relevant alternative for GPR and EMI data fusion. Sequential inversions of different configurations for a two layered medium show that in the case of high conductivity or permittivity for the first layer, the inversion scheme can not fully retrieve the soil hydrogeophysical parameters. But in the case of low permittivity and conductivity for the first layer, GPR–EMI inversion provides proper estimation of values compared to the EMI–GPR inversion.

Key words: Inverse theory; Ground penetrating radar; Magnetic and electrical properties; Hydrogeophysics.

1 INTRODUCTION

The shallow subsurface of the Earth is an extremely important geological zone, as it produces much of our water resources, supports our agriculture and ecosystems, affects our climate and sustains food production for humanity. The soil mediates many of the processes that govern water resources and quality, such as the partition of precipitation into infiltration and runoff, groundwater recharge, contaminant transport, plant growth, evaporation and energy exchanges between the Earth's surface and its atmosphere. As safe and effective use of subsurface environment is a challenge, there is a great need to improve our understanding of the soil and groundwater. In this respect, development of non-invasive characterization and monitoring techniques of the soil has become important. In particular, hydrogeophysical techniques are required to assess dynamic subsurface phenomena and to develop optimal sustainability, exploitation and remediation strategies.

Amongst existing geophysical techniques, ground penetrating radar (GPR) and electromagnetic induction (EMI) are of particular interest for providing high-resolution subsurface images and monitoring soil electrical properties. GPR is based on the transmission and reception of VHF–UHF (30–3000 MHz) electromagnetic waves into the ground. As the dielectric permittivity of water overwhelms the permittivity of other soil components, the presence of water in the soil principally governs GPR wave propagation. As a result, GPR-derived dielectric permittivity is usually used as a

surrogate measure for soil water content. In the areas of unsaturated zone hydrology and water resources, GPR has been used to identify soil stratigraphy (Grandjean *et al.* 2006), to locate water tables (Nakashima *et al.* 2001), to identify soil hydraulic parameters (Binley *et al.* 2002; Kowalsky *et al.* 2005), to measure soil water content (Huisman *et al.* 2003), to assess soil salinity (al Hagrey & Muller 2000), and to delineate soil compaction within agricultural fields (Petersen *et al.* 2005). EMI is widely used for proximal soil electrical conductivity determination based on the radiation of a VLF EM wave into the soil. Depending on soil electrical conductivity, eddy currents are generated and produce a secondary EM field which is then recorded by the EMI system. This method operates at frequencies ranging from 1–100 kHz. EMI applications are quite diversified, it is notably used for salinity mapping and monitoring in agricultural fields (Cameron *et al.* 1981; Hendrickx *et al.* 1992; Lesch *et al.* 1998; Amezketa 2006), soil water content estimation (Kachanoski *et al.* 1988; Reedy & Scanlon 2003; Sherlock & McDonnell 2003), soil texture mapping (Hedley *et al.* 2004; Triantafilis & Lesch 2005), soil acidity assessment (Dunn & Beecher 2007), detection of buried metallic bodies like unexploded ordnance (UXO) (Pasion *et al.* 2007; Huang & Won 2003), detection of contaminants in soils and shallow aquifers (Ladwig 1983; Hoekstra *et al.* 1992), clay content estimation (McBratney *et al.* 2005; Triantafilis & Lesch 2005) and characterization of the vadose zone (Everett *et al.* 2006).

It is possible to increase the information extracted from geophysical data by combining different geophysical sensors in an integrated inverse modelling scheme that may properly regularize the overall inverse estimation problem. For instance, Ghose & Slob (2006) combined GPR and seismic data to obtain unique estimates for water saturation and porosity in the soil. Lines *et al.* (1988) proposed two main approaches for cooperative inversion of geophysical data. The first one is joint inversion, in which multiple objective functions are combined into one overall objective function and the optimal solution is controlled by a weight vector. The choice of the respective weights of the two data sets is critical and constitutes the main difficulty of this method. Several weighting methods have been applied by different authors. The inverse of data variance as weighting vector is commonly used for multi-objective optimization. One of the first methods proposed for multi-objective optimization is Goal programming. In this approach, we define a goal or aspiration level (each measurement is given a goal or target value to be achieved) for each component of the objective function. Then, the distances between the goal vector and the objective function vector are minimized (Charnes & Cooper 1960). Zeleny (1982) also modified the goal programming technique using ideal point vector instead of goal vector, called ideal point method. In this approach, the ideal point vector is the minimum of the objective function vector. Another approach applied in joint inversion is Bayesian data fusion (Aster *et al.* 2005). This method sets the problem in a proper probabilistic framework and also provides a straightforward way to update existing probability density functions with new relevant information (Ezzedine *et al.* 1999; Chen *et al.* 2001; Chen & Rubin 2003; Bogaert & Fasbender 2007). Genetic algorithms have been recently used for geophysical data fusion (Srinivas & Deb 1994; Deb *et al.* 2002; Moorkamp *et al.* 2007), which use a population of points that are able to find multiple Pareto-optimal solutions simultaneously. A review of different methods applied for geophysical joint inversion is presented by Kozlovskaya *et al.* (2007). The second approach proposed by Lines *et al.* (1988) for cooperative inversion of geophysical data is sequential inversion in which the different data sets are inverted successively. The interest of this method is that it avoids from the weighting problem of the joint inversion.

Based on work by Lambot *et al.* (2004) and Moghadas *et al.* (2010), we investigated the effectiveness of different approaches for integrated inversion of off-ground GPR and EMI data. We first combined the GPR and EMI sources of information into a single objective function using two different techniques, namely, weighting by the inverse of the data variance and using ideal point method (Zeleny 1982; Kozlovskaya *et al.* 2007). The Bayesian method corresponds to the third studied technique, considering normality for the distribution of the parameter estimates. Finally, we performed sequential inversion using the information obtained from the inversion of the EMI data as *a priori* information to invert the GPR data, and vice versa.

2 MATERIALS AND METHODS

2.1 GPR and EMI forward models

For both GPR and EMI, antenna-subsurface modelling is based on the approach proposed by Lambot *et al.* (2004). In this method, a monostatic off-ground antenna is connected to a vector network analyser (VNA) playing the role of transmitter and receiver. A TEM horn antenna is used for the GPR measurements, while a loop antenna is used for EMI data acquisition. The advantage of VNA compared to traditional GPR and EMI systems is that the measured quantity, i.e. the ratio between received and transmitted signal, is physically well described and established as an international standard with robust calibration (Ferrero *et al.* 1994; Martens *et al.* 2005; Hiebel 2007).

Assuming the soil surface to be located in the far field region of the GPR antenna and the EMI loop antenna to be small compared to the wavelength in the air and skin-depth in the ground, the zero-offset antenna reduces to a point source and receiver. The point source and receiver is assumed to be located above a 3-D, horizontally multilayered medium. As the variations in the model configuration are only in one direction, the earth model is 1-D but the sources and receivers are 3-D. As a result, the wavefield propagation and modelling are 3-D using a 1-D earth model. The medium consists of N layers separated by $N-1$ planar interfaces parallel to the x–y plane of a right-handed Cartesian coordinate system. The medium of the nth layer is homogeneous and characterized by magnetic permeability μ_n, dielectric permittivity ε_n, electrical conductivity σ_n and thickness h_n.

Assuming the distribution of the electromagnetic field measured by the antenna to be independent of the distribution of the soil properties and antenna height, that is, only the phase and amplitude of the field change, any antenna can be modelled using the following equation (Lambot *et al.* 2004)

$$S_{11}(\omega) = \frac{b(\omega)}{a(\omega)} = H_i(\omega) + \frac{H(\omega)G^{\uparrow}_{**}(\omega)}{1 - H_f(\omega)G^{\uparrow}_{**}(\omega)}, \quad (1)$$

where $S_{11}(\omega)$ is the frequency-dependent quantity measured by the VNA, $b(\omega)$ and $a(\omega)$ are, respectively, the received and emitted waves, ω is the angular frequency, $H_i(\omega)$, $H(\omega)$ and $H_f(\omega)$ are the characteristic antenna transfer functions accounting for all multiples in the antenna and between the antenna and the soil, and $G^{\uparrow}_{**}$ is the Green's function of the air–subsurface system modelled as a 3-D multilayered medium. The Green's function for GPR ($G^{\uparrow}_{xx}$) is defined as the backscattered x-directed electric field at the antenna phase centre for a unit x-directed electric source situated also at the

antenna phase centre. The Green's function for EMI ($G_{zz}^{\uparrow}$) is defined as the backscattered z-directed magnetic field at the antenna phase centre for a unit z-directed magnetic source situated also at the antenna phase centre.

The spatial-domain Green's function for GPR is found to be (Lambot *et al.* 2004)

$$G_{xx}^{\uparrow} = \int_0^{+\infty} \tilde{G}_{xx}^{\uparrow}(k_\rho) k_\rho \mathrm{d}k_\rho, \tag{2}$$

where the spectral Green's function is defined as

$$\tilde{G}_{xx}^{\uparrow}(k_\rho) = \frac{1}{8\pi}\left(\frac{\Gamma_1 R_1^{\mathrm{TM}}}{\eta_1} - \frac{\zeta_1 R_1^{\mathrm{TE}}}{\Gamma_1}\right)\exp(-2\Gamma_1 h_1). \tag{3}$$

In this expression, the subscripts denote layer indexes, R^{TE} and R^{TM} are respectively, the transverse electric (TE) and transverse magnetic (TM) global reflection coefficients accounting for all reflections and multiples from inferior interfaces, Γ is vertical wavenumber defined as $\Gamma = \sqrt{k_\rho^2 - k^2}$, whilst $k^2 = \omega^2\mu(\varepsilon - \frac{\jmath\sigma}{\omega})$, $\zeta_1 = \jmath\omega\mu_1$ and $\eta_1 = \sigma_1 + \jmath\omega\varepsilon_1$. For the free-space layer 1, we have $k_1^2 = (\frac{\omega}{c})^2$ in which c is the speed of light in free space. Similarly, the spatial-domain Green's function for EMI is defined as (Moghadas *et al.* 2010)

$$G_{zz}^{\uparrow} = \int_0^{+\infty} \tilde{G}_{zz}^{\uparrow}(k_\rho) k_\rho \mathrm{d}k_\rho, \tag{4}$$

for which the spectral Green's function is found to be

$$\tilde{G}_{zz}^{\uparrow}(k_\rho) = \left(\frac{k_\rho^2 R_1^{\mathrm{TE}}}{4\pi\zeta_1\Gamma_1}\right)\exp(-2\Gamma_1 h_1). \tag{5}$$

The transformation back to the spatial domain Green's function is performed by a fast integral evaluation technique. The proposed integration paths for GPR and EMI are discussed in detail in Lambot *et al.* (2007) and Moghadas *et al.* (2010), respectively.

2.2 Model inversion

The soil layer constitutive parameters and thicknesses are obtained from EMI and GPR data inversion, resulting in a non-linear optimization problem. Parameter vector $\mathbf{b} = [\varepsilon_n, \sigma_n, h_n]$ ($n = 1, \ldots, N$) is determined minimizing an objective function $\phi(\mathbf{b})$. In the particular case where no prior information on the parameters is taken into account and assuming observation errors to be normally distributed, the maximum likelihood theory reduces to the classical least squares problem (Carrera & Neuman 1986). For GPR and EMI taken separately, the objective function is defined as follows:

$$\phi(\mathbf{b}) = \left(\mathbf{G}_{**}^{\uparrow\mathbf{meas}} - \mathbf{G}_{**}^{\uparrow\mathbf{mod}}\right)^{\dagger} \mathbf{C}^{-1} \left(\mathbf{G}_{**}^{\uparrow\mathbf{meas}} - \mathbf{G}_{**}^{\uparrow\mathbf{mod}}\right), \tag{6}$$

where $G_{**}^{\uparrow\mathrm{meas}} = G_{**}^{\uparrow\mathrm{meas}}(\omega)$ and $G_{**}^{\uparrow\mathrm{mod}} = G_{**}^{\uparrow\mathrm{mod}}(\omega, \mathbf{b})$ are the measured and modelled GPR or EMI Green's functions, respectively, $\mathbf{C}$ is the measurement error covariance matrix and $\mathbf{b}$ is the parameter vector to be optimized, which includes the layer electromagnetic properties and thicknesses. In most electromagnetic problems, this function is non-linear which necessitates using robust global optimization algorithms. The minimization of eq. (6) is carried out using the global multilevel coordinate search (GMCS) algorithm (Huyer & Neumaier 1999) combined sequentially with the classical Nelder–Mead simplex (NMS) algorithm (Lagarias *et al.* 1998).

The GMCS is a global method robust in finding minimum of the multidimensional non-linear objective functions with complex topography without requiring excessive computing resources. In contrast to many stochastic methods that operate only at the global level and are therefore quite slow, this approach has quick convergence particularly, when the objective function is continuous in the neighbourhood of the global minimum. Furthermore, GMCS does not need to calculate derivatives of the objective function, causing it to be very insensitive to possible discontinuity of the objective function. The NMS algorithm is a non-linear fast local search method that does not need to calculate an explicit formulation of the objective function Jacobian. In other words, this method attempts to minimize a scalar-valued non-linear function of n real variables using only function values, without any derivative information. An extensive review about both optimization techniques and in particular, their applications for soil hydraulic properties estimations can be found in Lambot *et al.* (2002).

2.3 Data fusion

The estimation of the soil dielectric permittivity and electrical conductivity are important, but until now it has been difficult to estimate them reliably from non-invasive geophysical sensors. Operating in the high frequencies, GPR essentially provides information about the dielectric permittivity. EMI uses a low frequency band and is mainly sensitive to the electrical conductivity. We integrated GPR and EMI data in order to fully take advantage of the complementary information provided by both methods in reconstructing multilayered media. This is useful when the conductivity is frequency independent or when other independent data sources give information about frequency dependence. When conductivity has frequency dependence, EMI and GPR data fusion is possible if the frequency dependence is known from EMI up to GPR frequencies. Due to the different operating frequency ranges of EMI and GPR and also different sampling volumes and sensitivities, the way such data fusion should be performed is not straightforward.

Indeed, the apparent electrical conductivity (including dielectric losses) of soils in the EMI–GPR frequency range is frequency dependent. As a result, in practice, a single electrical conductivity parameter will not be sufficient to describe the soil and an appropriate frequency dependence model has to be used, thereby involving additional parameters to optimize. This inherently complicates the inverse problem, but knowing frequency dependence also provides additional valuable information regarding the soil, and in particular regarding its texture (especially clay). Conceiving both joint and sequential inversion approaches, several multi-objective optimization techniques were considered.

2.3.1 Weighting methods

Our first approach consisted of defining a single objective function, corresponding to a weighted combination of the individual GPR and EMI objective functions (see eq. 6). The choice of the weights is of prime importance as it regulates the topography of the final objective function, thereby influencing the uniqueness and stability of the inverse solution and the accuracy of the parameter estimates. We applied a commonly used method using the inverse of the data variance as normalization (Simunek *et al.* 1998)

$$\phi_1 = \frac{\phi_{xx}}{\mathrm{var}\left|G_{xx}^{\uparrow\mathrm{meas}}\right|} + \frac{\phi_{zz}}{\mathrm{var}\left|G_{zz}^{\uparrow\mathrm{meas}}\right|}, \tag{7}$$

where subscripts xx and zz denote GPR and EMI, respectively.

As a second weighting technique, we employed the ideal point method. One of the first methods proposed for multi-objective optimization is Goal programming. In this approach, a goal or

aspiration level is defined for each component of the objective function. Then, the distances between the goal vector and the objective function vector are minimized (Charnes & Cooper 1960). A modification of the goal programming method is known as the ideal point method. The optimal value of the objective function is regarded as the ideal point in a multiple objective decision-making ideal point method. Appointing the weights using normalization to a distance between maximum and minimum values of each objective function, ideal point is formulated as follows (Zeleny 1982; Kozlovskaya *et al.* 2007):

$$\phi_2 = \frac{\phi_{xx} - \min(\phi_{xx})}{\max(\phi_{xx}) - \min(\phi_{xx})} + \frac{\phi_{zz} - \min(\phi_{zz})}{\max(\phi_{zz}) - \min(\phi_{zz})}. \quad (8)$$

Any solution to this problem is Pareto optimal. The Pareto optimality provides us a set of solutions called the Pareto-optimal set, characterized by the fact that starting from a solution within the set, one objective function can only be improved when at least one other objective function being deteriorated (Vrugt & Robinson 2007; Vrugt *et al.* 2007). This function cannot be easily used because normally we do not know the minimum and maximum values of the objective function from real data, unless the objective function is fully computed. Yet, the minimum value should tend to zero and, if the parameter space is sufficiently large, the maximum value is expected to occur at the corners of the domain and can therefore be readily calculated. It is worth noting that this fact is only valid when we are dealing with the simple case of a one-layered medium for which the relationship between soil electrical properties and the fields has a monotonic behaviour. When considering more layers, the objective function is highly non-linear and it is not ensured that the maximum is encountered at the corners of the parameter domain. In that case, the mean values between the corners can be considered.

2.3.2 Bayesian method

We also applied naive Bayesian data fusion to combine GPR and EMI information. In this approach, the measured quantity is a random variable, and the solution is a probability distribution for the model parameters. The Bayesian framework allows to naturally incorporate prior information about the solution that comes from other data or experiment, expressed as prior distribution. The data are combined with the prior distribution using Bayes' theorem to produce a posterior distribution for the model parameters. We assumed Gaussian conditional probability density functions for the parameters. In this case, the mean and the variance of the jointed GPR and EMI solution can be evinced as follows, respectively (Bogaert & Fasbender 2007)

$$m = \sum_{j=1}^{2} \frac{1/s_j^2}{\sum_{k=1}^{2} \left(1/s_k^2\right)} m_j, \quad (9)$$

$$s^2 = \frac{1}{\sum_{j=1}^{2} \frac{1}{s_j^2}}, \quad (10)$$

where m_j ($j = 1, 2$) are the individual parameter estimates for GPR and EMI and s_j^2 ($j = 1, 2$) are their corresponding variances. The variances s_j^2 are estimated from the Jacobian matrix around the minimum of the GPR and EMI objective functions (Kool & Parker 1988).

2.3.3 Sequential inversion

While the joint inversion approach weights the set of data and places them into one data vector, sequential inversion considers the sets of data separately. Averting from the weighting problem of the joint inversion scheme, sequential inversion was implemented as a final approach. First, we used the data obtained by EMI inversion as the input of GPR inversion algorithm (called EMI–GPR inversion). We also repeated the sequential inversion fixing the thickness and conductivity of the first and second layer for GPR inversion, respectively. We performed the same procedure considering the *a posteriori* information resulting from the inversion of the GPR data set as *a priori* information to invert the EMI data set (called GPR–EMI inversion). In this case, we repeated the method fixing the thickness and electrical permittivity of the fist layer for the EMI inversion. In all cases, we considered the height of the antenna above the surface as a fixed value.

3 NUMERICAL EXPERIMENTS AND RESULTS

3.1 Model configuration and synthetic data

Four synthetic GPR and EMI data sets were generated for a two layered medium as depicted in Fig. 1. The first data set is characterized by low electrical permittivity and conductivity values for the first layer ($\varepsilon_{r,1} = 9$ and $\sigma_1 = 10^{-2}\,\mathrm{S\,m^{-1}}$) and high corresponding values for the second layer ($\varepsilon_{r,2} = 15$ and $\sigma_2 = 10^{-1}\,\mathrm{S\,m^{-1}}$). The second data set presented the same values for electrical conductivities for both layers, while the electrical permittivities of the first and the second layers were reversed. Inversely, for the third data set, the electrical permittivity values of both layers were identical to that of the first data set, but with reversed configuration for the layer electrical conductivities. Finally, the fourth investigated data set presented higher values of both parameters for the first than for the second layer. For all data sets, the top layer thickness was set to $h_1 = 0.15$ m. The height of the antenna above the soil surface was fixed to $h_0 = 0.2$ m, and the magnetic permeability μ of the air and soil layers were considered as constant and equal to the free space permeability $\mu_0 = 4\pi \times 10^{-7}\,\mathrm{Hm^{-1}}$. Hence, the parameter vector **b** to be inverted for is defined as $\mathbf{b} = [\varepsilon_{r,1}, \varepsilon_{r,2}, \log_{10}(\sigma_1), \log_{10}(\sigma_2), h_1]$. The frequencies for EMI ranged from 1 to 50 kHz and for GPR the frequencies ranged from 800 to 2600 MHz, with frequency steps of 1 kHz and 6 MHz, respectively.

In order to assess the sensitivity of the data fusion approaches to the presence of noise and evaluate the applicability of these methods for a real case scenario, we introduced some noise in the data.

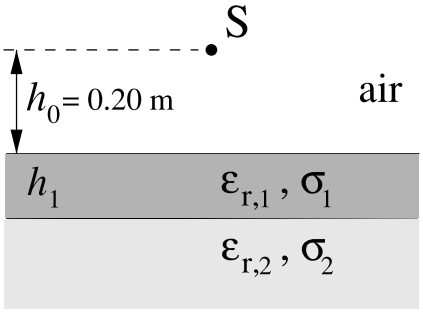

Figure 1. Model configuration: 3-D layered medium with the source **S** in air above two soil layers, including the lower half-space.

Considering all data sets, we added a Gaussian (standard normal distribution) random noise of 1 and 5 per cent to the average amplitude of $G^{\uparrow}_{zz}$ and $G^{\uparrow}_{xx}$, respectively. Fig. 2 illustrates the amplitude of the Green's function for EMI and GPR data conceiving the four different configurations with a Gaussian random noise added to them.

3.2 Weighting methods

Projections of the objective functions on key parameter planes crossing the actual parameter values are presented in Fig. 3 for the investigated formulations, considering GPR and EMI data (applying the first data set) separately and jointly. The analysis of the objective function topography is important as it provides valuable insights into the uniqueness of the inverse solution, the sensitivity of the model to the different parameters, and parameter correlations. In the $\varepsilon_{r,1}-\varepsilon_{r,2}$ parameter plane, the objective function for EMI presents a minimum quite different from the real value (Fig. 3a), resulting from the low sensitivity of EMI with respect to the soil dielectric permittivity. For GPR (Fig. 3b) the global minimum is much well defined and unique. Weighting the integrated objective function by the inverse of the variance of the data (ϕ_1) and also the second objective function (ϕ_2) result logically in objective functions almost identical to the GPR one (Figs 3c and d).

In the $\varepsilon_{r,1} - \sigma_1$ plane, we clearly observe the high sensitivity of EMI to electrical conductivity, while it is not sensitive to dielectric permittivity (Fig. 3e). In contrast, GPR presents a better sensitivity to dielectric permittivity and less to electrical conductivity (Fig. 3f). Combining GPR and EMI information appears quite relevant for proper estimation of these parameters. The first combination of EMI and GPR data (Fig. 3g) leads to a well defined minimum, which is advantageous in terms of uncertainty for the estimation of both parameters. For the second formulation (Fig. 3h), the global minimum is much well defined, although the topography suffers from flatness in the permittivity and conductivity directions.

In the $\varepsilon_{r,2}$–σ_1 plane, results for EMI are quite similar to that observed for the preceding parameter plane (Fig. 3i), while a positive correlation between the two parameters is observed for GPR (Fig. 3j). This correlation is to be attributed to the fact that no traveltime information is available to constrain $\varepsilon_{r,2}$. This parameter is therefore can only be obtained through the reflection coefficient. Yet, the reflection strength increases with either higher values of $\varepsilon_{r,2}$ or lower values of σ_1. Here again, the objective function obtained from weighting by the inverse of the data variance is well defined. For the ideal point formulation, the minimum is better defined than that of the EMI and GPR individual response functions, while some flatness is still observed around it (Fig. 3l).

In the $\varepsilon_{r,1}$–h_1 plane, the EMI minimum is quite well defined for h_1, while the response function presents a flat valley in the direction of the dielectric permittivity (Fig. 3m). For GPR, the objective function is much flatter (Fig. 3n). Moreover, a negative correlation is observed between both parameters, which is due to the fact that, considering the propagation time information in the GPR data, increasing the top layer thickness will lead to the same effect (increased propagation time) as increasing the dielectric permittivity (decreasing wave velocity). The correlation is however not entire, as the amplitude information permits to regularize to some extent that ambiguity. Weighting EMI and GPR information by the inverse of the data variances results in a rather flat region around the minimum, especially in the $\varepsilon_{r,1}$ direction (Fig. 3o), while the EMI information clearly dominates in the ideal point response function (Fig. 3p).

Finally, in the σ_1–σ_2 parameter plane, a very high negative correlation between the two parameters is observed for EMI (Fig. 3q). This shows that EMI is almost equally sensitive to both layers for that model configuration and the layers can therefore not easily be separated from the EMI data alone. In contrast, GPR provides a better defined minimum (Fig. 3r), which is further constrained by integrating GPR and EMI data using ϕ_2 (Fig. 3t). As well in this case, weighting the data by the inverse of their variance did not lead to proper data fusion (Fig. 3s).

3.3 Bayesian data fusion

Bayesian data fusion relies on the probability density of the data and sets the problem in a proper probabilistic framework. This method also provides a straightforward way to update existing probability density functions with new relevant information. Fig. 4 shows the results of the Bayesian data fusion of GPR and EMI data (employing the first data set) corresponding to each pair of parameters examined above for the weighting methods (see Section 3.2), setting the other parameters to their true value. We assumed normal probability density functions for the parameter estimates. For the $\varepsilon_{r,1}-\varepsilon_{r,2}$ pair (Fig. 4a), we observe a flat distribution of both parameters estimated from EMI data, explained by the flat topography of the objective function in the corresponding plane (see Fig. 3a) and the resulting large parameter variance estimates ($s^2_{\varepsilon_{r,1}} = 8 \times 10^7$ and $s^2_{\varepsilon_{r,2}} = 6 \times 10^7$). In contrast, for GPR, the better definition of the minimum provides much more accurate parameter estimates ($\varepsilon_{r,1} = 8.9$ and $\varepsilon_{r,2} = 14.9$). As a result of weighting by the inverse of the variances of parameter estimations in Bayesian data fusion (see eq. 9), EMI estimates have negligible contributions in the definition of the Bayesian parameter distributions, which are therefore superimposed to those for GPR. Quite similar results, arising from a lack of sensitivity of EMI to permittivity, are observed in all the other cases concerned with estimation of this parameter (Figs 4b–d).

For the $\varepsilon_{r,1}$–σ_1 pair (Fig. 4b), the well defined minimum of the EMI objective function in the direction of the electrical conductivity (see Fig. 3e) leads to an accurate estimation of this parameter ($\sigma_1 = 10^{-2}\,\mathrm{S\,m^{-1}}$), with an estimated variance lower than that from GPR (for EMI: $s^2_{\sigma_1} = 6 \times 10^{-4}$ and for GPR: $s^2_{\sigma_1} = 8 \times 10^{-2}$). Therefore, in this case, information from EMI dominates in the definition of the Bayesian Gaussian distribution. Comparable results are observed for the $\varepsilon_{r,2}-\sigma_1$ pair (Fig. 4c). The low contribution of GPR originates from the large uncertainty in the estimation of electrical conductivity associated with the flatness of the response function in the direction of this parameter (see Fig. 3j).

Concerning the $\varepsilon_{r,1}$–h_1 pair (Fig. 4d), inversion of GPR data leads to inaccurate estimates of the first layer thickness ($h_1 = 3$ m). In contrast, EMI dominates the Bayesian inversion with accurate estimation of h_1 (=0.15 m), due to the valley in EMI objective function in that direction (Fig. 3m). Therefore, both EMI and Bayesian present a low variance around the real h_1 value (for both EMI and Bayesian: $s^2_{h_1} = 2.3 \times 10^{-6}$). Regarding the σ_1–σ_2 pair (Fig. 4e), the strong correlation observed between both parameters in the EMI response function for this model configuration, and the resulting flatness of the minimum region (see Fig. 3q), does not allow simultaneous accurate estimations of electrical conductivities of the two layers using EMI alone. Therefore, GPR essentially contributes to the Bayesian estimate of σ_1, for which the minimum is better defined (see Fig. 3r).

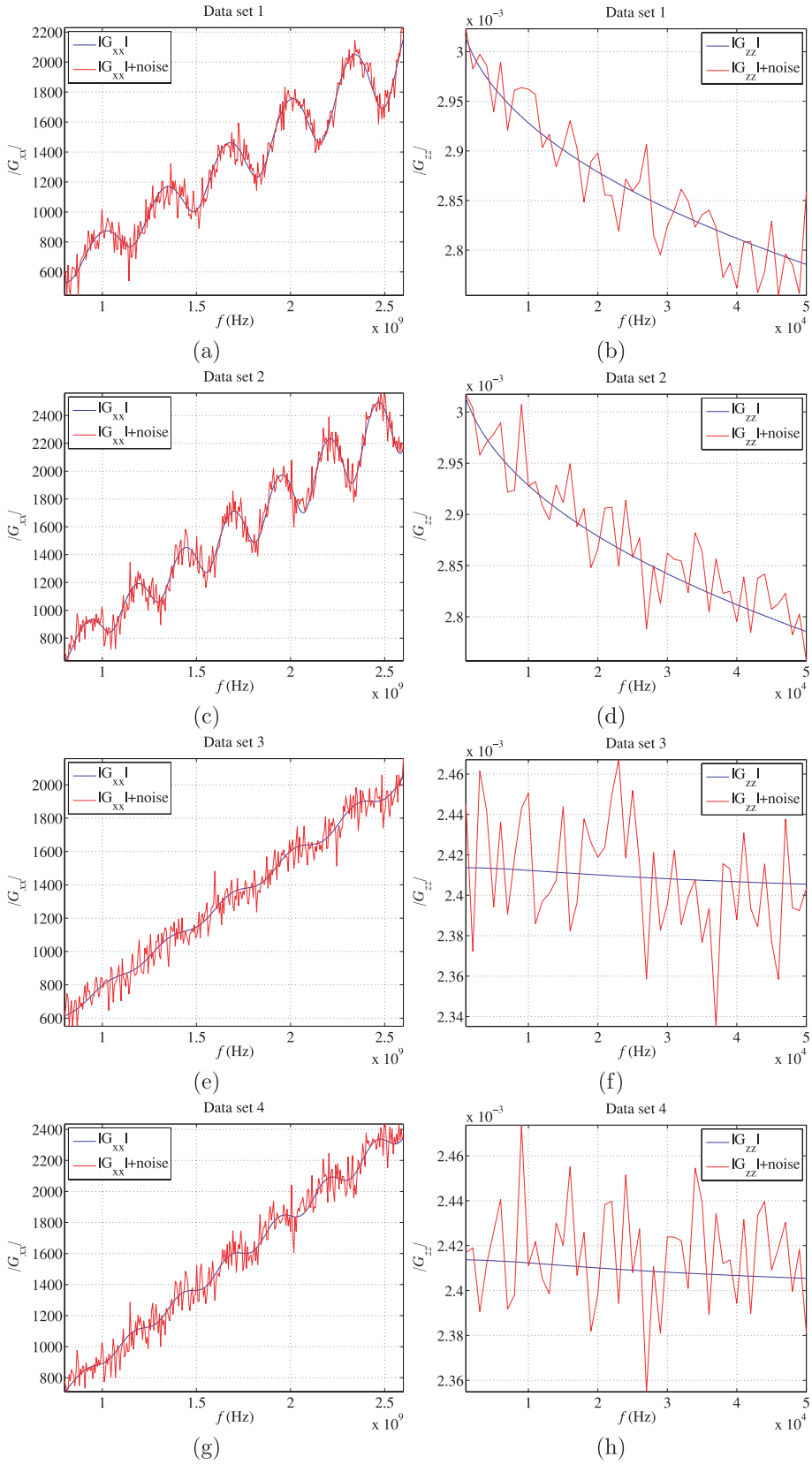

Figure 2. Gaussian random noise (red plots) added to the data (blue plots) for four deferent data sets. Left-handed plots show the amplitude of GPR Green's function and the right handed plots correspond to the amplitude of EMI Green's function. For all configurations, we added a Gaussian (standard normal distribution) random noise of 1 and 5 per cent to the average amplitude of $G_{zz}^{\uparrow}$ and $G_{xx}^{\uparrow}$, respectively.

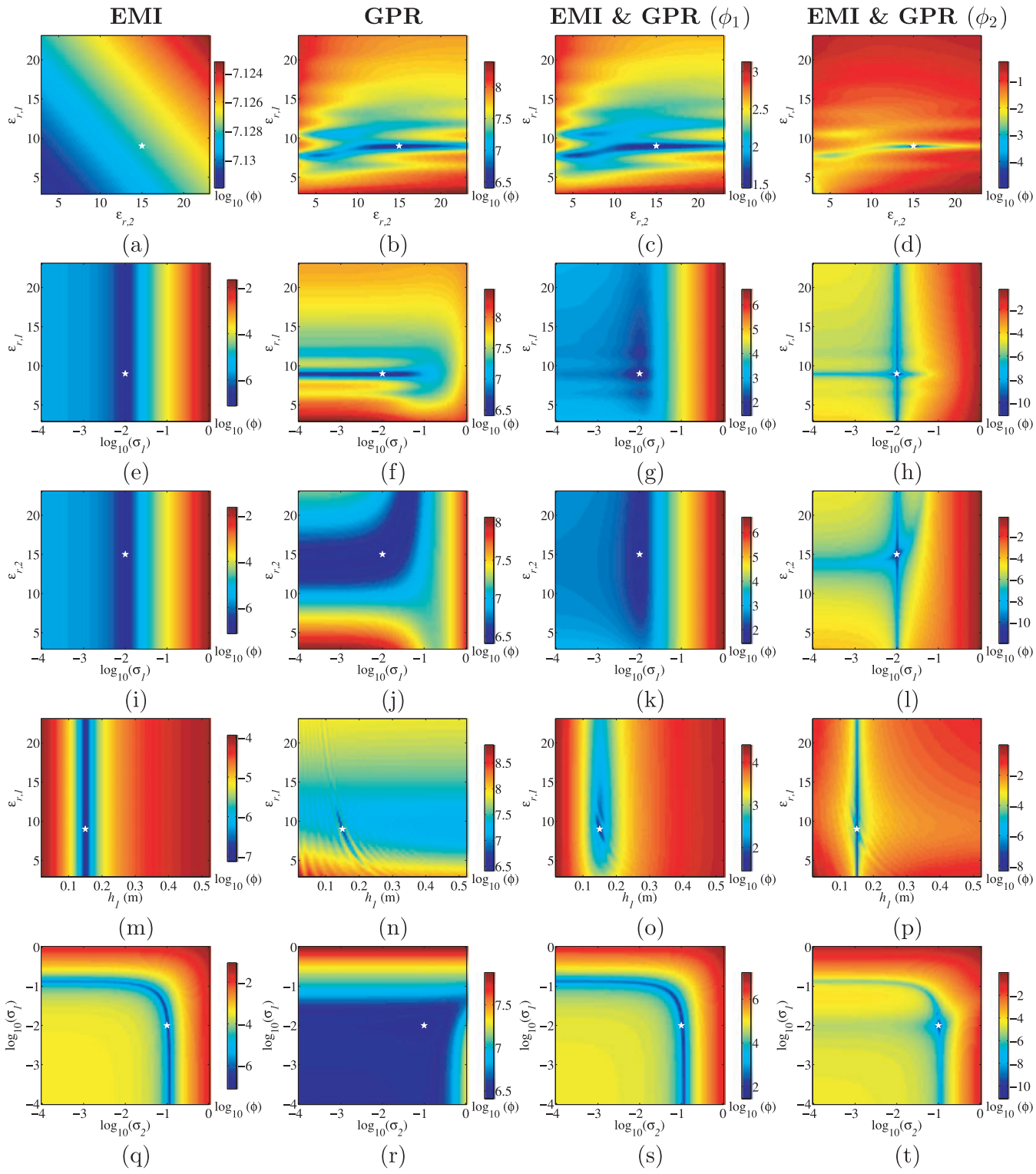

Figure 3. Response surfaces of the objective function for different formulations, considering GPR and EMI data separately and jointly, and different parameter planes of the full 5-D objective function. The white star represents the true values of the parameters.

3.4 Sequential inversion

As a fourth joint optimization technique, we implemented sequential inversion. We compared the EMI–GPR sequential inversion procedure, in which EMI parameter estimates were used as initial guess values for GPR data optimization, with GPR–EMI sequential inversion scheme for which GPR and EMI data are inverted consecutively. Furthermore, two strategies were considered in each case, either inverting both EMI and GPR data for all investigated parameters (complete sequential inversion strategy) or performing the second sequential inversion step fixing some parameter values to their estimate from the first step (partial sequential inversion

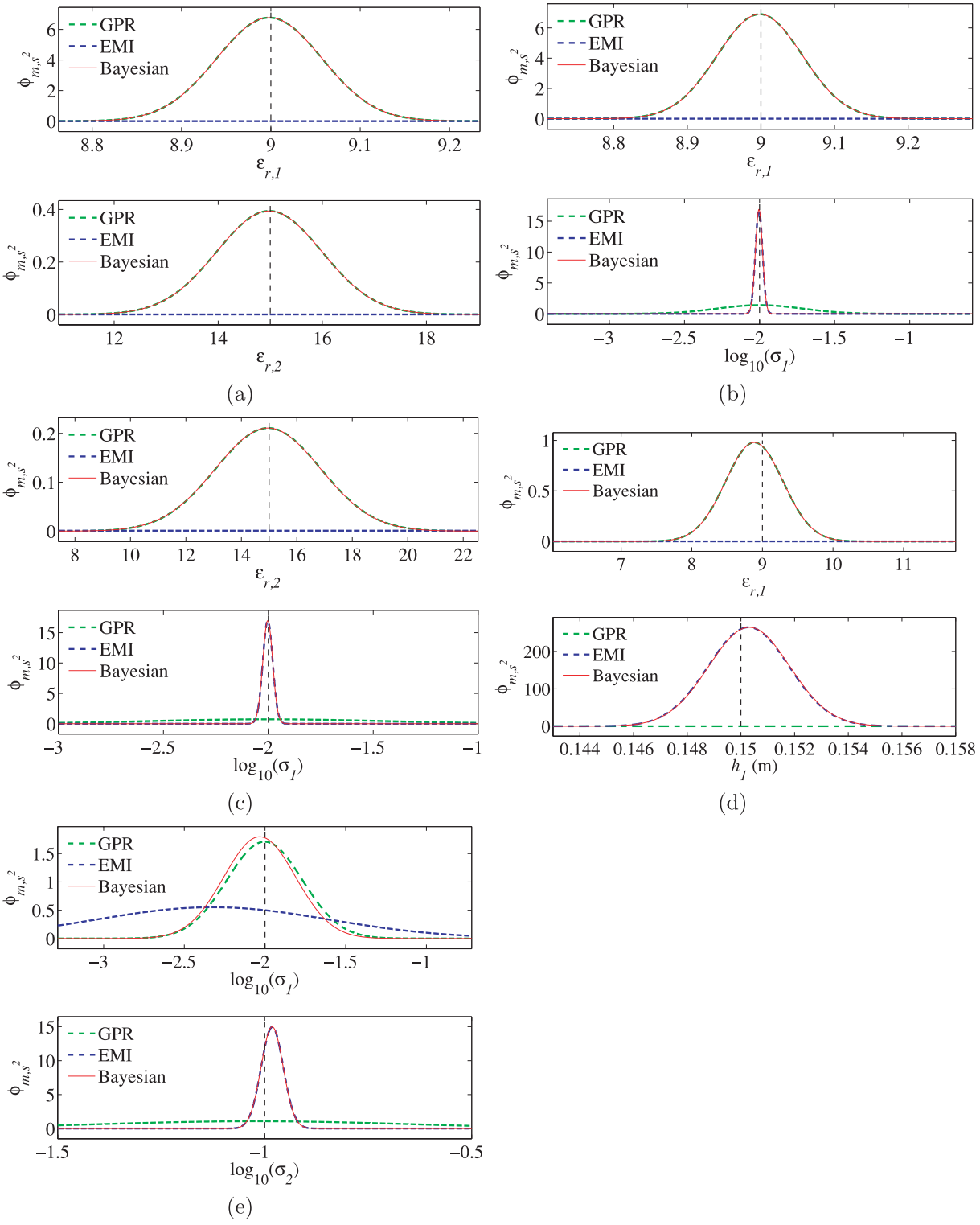

Figure 4. Gaussian distribution of value parameters, considering GPR and EMI data separately and jointly. The black dashed line shows the real value.

strategy). More specifically for this latter strategy, partial EMI–GPR inversion was carried out optimizing GPR data for $\varepsilon_{r,1}$, $\varepsilon_{r,2}$ and σ_1 only, fixing values of h_1 and σ_2 to EMI estimates. In contrast, partial GPR–EMI inversion was performed considering GPR estimates for h_1 and $\varepsilon_{r,1}$ as fixed values for EMI data inversion. In order to investigate the efficiency of sequential inversion for different hydrogeophysical properties, each of these approaches was applied on several synthetic data sets generated for two-layered media with contrasted electrical property configurations (see Table 1). The height of the antenna above the soil surface was equal to $h_0 =$ 0.20 m and it was considered as a fixed parameter in all sequential inversion strategies. The results are presented in Table 1.

For the first data set, parameter estimates obtained from complete EMI–GPR inversion differ generally strongly from the

Table 1. Estimations of two-layered medium properties from several sequential inversion techniques for four contrasted electrical property configurations.

		EMIGPR inversion				GPR-EMI inversion			
		Complete		Partial		Complete		Partial	
		EMI	GPR	EMI	GPR	GPR	EMI	GPR	EMI
Data set 1									
$\varepsilon_{r,1}$	9	3652.08	4625.75	3652.08	9.14	9.06	9.34	9.06	9.06
$\varepsilon_{r,2}$	15	−2699.52	−3170.30	−2699.52	7.81	14.53	15.00	14.53	−54.99
h_1	0.15	0.12	0.10	0.12	0.12	0.15	0.15	0.15	0.15
$\log(\sigma_1)$	−2	−3.83	−3.38	−3.83	−1.51	−2.22	−2.27	−2.22	−2.23
$\log(\sigma_2)$	−1	−1.01	−0.67	−1.01	−1.01	−1.09	−0.98	−1.09	−0.99
Data set 2									
$\varepsilon_{r,1}$	15	−332.13	14.98	−332.13	14.76	14.98	34.56	14.98	14.98
$\varepsilon_{r,2}$	9	−7.55	13.20	−7.55	17.12	13.87	−1.51	13.87	−516.15
h_1	0.15	0.13	0.21	0.13	0.13	0.24	0.15	0.24	0.24
$\log(\sigma_1)$	−2	−2.25	−1.48	−2.25	−1.65	−1.52	−2.07	−1.52	−1.48
$\log(\sigma_2)$	−1	−1.02	−1.98	−1.02	−1.02	−1.05	−1.00	−1.05	−1.02
Data set 3									
$\varepsilon_{r,1}$	9	12.12	8.87	12.12	8.83	8.85	8.58	8.85	8.85
$\varepsilon_{r,2}$	15	92.52	10.99	92.52	8.89	2.89	2.88	2.89	248.50
h_1	0.15	0.06	0.13	0.06	0.06	0.32	0.30	0.32	0.32
$\log(\sigma_1)$	−1	−0.79	−0.99	−0.79	−0.99	−0.98	−1.09	−0.98	−1.14
$\log(\sigma_2)$	−2	−1.92	−2.91	−1.92	−1.92	−12.04	−12.43	−12.04	−1.96
Data set 4									
$\varepsilon_{r,1}$	15	−40.22	15.04	−40.22	15.24	15.04	14.55	15.04	15.04
$\varepsilon_{r,2}$	9	16.05	−6.56	16.05	21.94	6.85	6.85	6.85	14.85
h_1	0.15	0.14	0.82	0.14	0.14	0.34	0.32	0.34	0.34
$\log(\sigma_1)$	−1	−1.00	−0.95	−1.00	−0.99	−0.95	−1.10	−0.95	−1.15
$\log(\sigma_2)$	−2	−1.89	1.83	−1.89	−1.89	−12.16	−12.48	−12.16	−1.94

Notes: In the EMI–GPR inversion scheme, EMI parameter estimates are used as guess values for the GPR data optimization, and inversely for the GPR–EMI scheme. The complete inversion strategy corresponds to inversion of both EMI and GPR data for all the parameters. For the partial EMI–GPR strategy, GPR data are inverted fixing parameters h_1 and σ_2 to their EMI estimates. For the partial GPR–EMI strategy, EMI data are optimized considering h_1 and $\varepsilon_{r,1}$ as fixed to their GPR estimates.

theoretical values ($\varepsilon_{r,1} = 4625.75$, $\varepsilon_{r,2} = -3170.30$, $h_1 = 0.10$ m, $\sigma_1 = 10^{-3.38}\,\mathrm{S\,m^{-1}}$ and $\sigma_2 = 10^{-0.67}\,\mathrm{S\,m^{-1}}$). These observations result from non-uniqueness issue in the inverse problem, notably due to the low information content of EMI data with respect to the both layer permittivities (see Figs 3a, e, i and m) associated with the relatively low sensitivity of GPR to $\varepsilon_{r,2}$ and its correlation with σ_1 (see Figs 3b, f and j). Considering two EMI highly sensitive parameters (i.e. h_1 and σ_2) as fixed values for GPR optimization, partial EMI–GPR sequential inversion allows to better constraint the inverse problem and generally leads to much more reliable parameter estimations, particularly for the permittivity and conductivity of the first and second layer, respectively ($\varepsilon_{r,1} = 9.14$ and $\sigma_2 = 10^{-1.01}\,\mathrm{S\,m^{-1}}$). As a result of generally better defined minima of the GPR objective function compared with EMI for this data set (see Fig. 3), complete GPR–EMI sequential inversion provides estimates almost corresponding to the theoretical values for all parameters ($\varepsilon_{r,1} = 9.34$, $\varepsilon_{r,2} = 15$, $h_1 = 0.15$ m, $\sigma_1 = 10^{-2.27}\,\mathrm{S\,m^{-1}}$ and $\sigma_2 = 10^{-0.98}\,\mathrm{S\,m^{-1}}$). Partial GPR–EMI inversion also improves the estimation of all parameters except electrical permittivity of the second layer in which the sequential inversion scheme detriments the prediction ($\varepsilon_{r,2} = -54.99$). This configuration characterized by low electrical conductivity and permittivity values for the first layer which is favourable to high penetration depth of the electromagnetic fields. Therefore, in this case, both GPR and EMI techniques allows to retrieve rather accurate information for the two layers. This fact postulates to study the effects of different data set configurations on this approach.

Regarding the second data set, complete EMI–GPR sequential inversion leads to parameter estimates quite different from the expected theoretical values, except for the permittivity of the first layer ($\varepsilon_{r,1} = 14.98$). Partial EMI–GPR sequential inversion allows to properly estimate σ_2 ($=10^{-1.02}\,\mathrm{S\,m^{-1}}$) in addition to $\varepsilon_{r,1}$($=14.76$), while the estimations for the three other parameters remain quite apart from the real values ($\varepsilon_{r,2} = 17.12$, $h_1 = 0.13$ m and $\sigma_1 = 10^{-1.65}\,\mathrm{S\,m^{-1}}$). This is because of the flat topography of the EMI objective functions for these parameters, in particular for permittivity of the second layer. Complete GPR–EMI sequential inversion estimates $h_1 = 0.15$ m, $\sigma_1 = 10^{-2.07}\,\mathrm{S\,m^{-1}}$ and $\sigma_2 = 10^{-1}\,\mathrm{S\,m^{-1}}$ corresponding to their real values but presents inaccurate estimates for $\varepsilon_{r,1}$($=34.56$) and $\varepsilon_{r,2}$($=-1.51$). Partial GPR–EMI sequential inversion fails to retrieve the conductivity and permittivity of the first and second layer, respectively ($\sigma_1 = 10^{-1.48}\,\mathrm{S\,m^{-1}}$ and $\varepsilon_{r,2} = -516.15$) but provides accurate estimates for $\varepsilon_{r,1}$($=14.98$) and $\sigma_2 = 10^{-1.02}\,\mathrm{S\,m^{-1}}$. The general failing of the methods for retrieving the values for $\varepsilon_{r,2}$ arises from the high permittivity of the first layer and consequently, low penetration of the GPR signal in the second layer. In contrast, the low conductivity of the first layer (allowing higher EMI penetration depth) contributes to rather good estimations for the electrical conductivity of both layers.

For the third scenario, the value obtained for $\varepsilon_{r,2}$ from complete EMI–GPR inversion shows deviation from the corresponding real value ($\varepsilon_{r,2} = 10.99$) resulting from the flat topography of the EMI objective function around permittivity of the second layer. Partial EMI–GPR inversion considerably improves the estimation

Table 2. Calculation time for inversion of EMI and GPR data separately and sequentially for four different configurations.

		Calculation time (s)					
		EMI–GPR inversion			GPR–EMI inversion		
		EMI	GPR	EMI–GPR	GPR	EMI	GPR–EMI
Data set 1	Complete	1726	121	1847	260	52	312
	Partial	1530	280	1810	414	423	837
Data set 2	Complete	1828	63	1891	445	263	708
	Partial	1727	267	1993	462	758	1220
Data set 3	Complete	1330	32	1361	488	4	492
	Partial	1916	82	1998	642	492	1134
Data set 4	Complete	2111	25	2136	464	5	470
	Partial	2017	72	2089	531	692	1223

Note: The time for sequential inversions are presented for both partial and complete inversions.

of σ_2 ($=10^{-1.92}$ S m^{-1}), while it again fails to retrieve $\varepsilon_{r,2}$(=8.89). Estimation of the permittivity of the second layer obtained from complete GPR–EMI inversion differs from the theoretical value by 80 per cent but the obtained results for conductivity and permittivity of the first layer are quite close to the real values ($\varepsilon_{r,1} = 8.58$ and $\sigma_1 = 10^{-1.09}$ S m^{-1}). Partial GPR–EMI inversion also fails to retrieve the permittivity of the second layer ($\varepsilon_{r,2} = 248.50$). As a result of the high electrical conductivity of the first layer in this configuration, electromagnetic wave has a low penetration depth into the subsurface. This explains the failure of the investigated sequential inversion methods in retrieving $\varepsilon_{r,2}$.

For the last data set, high values for the dielectric permittivity and for the electrical conductivity of the first layer both induce low penetration depth of the magnetic waves in the subsurface. This again explains the generally large deviations of the $\varepsilon_{r,2}$ estimates from the theoretical values for the different sequential inversion schemes, as well as the low efficiency of GPR to retrieve h_1 in the all inversion strategies. In contrast, electrical conductivities of both layers are well estimated in all cases, except for the complete GPR–EMI inversion failing to retrieve σ_2 ($=10^{-12.48}$ S m^{-1}).

Table 2 presents the calculation time for EMI and GPR inversions separately and sequentially. GPR inversions are faster than EMI inversions which is because of the integration path and oscillations of EMI integrand in spatial domain Green's function (Lambot *et al.* 2007; Moghadas *et al.* 2010). Due to the topography of the objective functions in the complete sequential inversions, we only used local optimization for the second inversion scheme. As a result, in most scenarios, partial inversions consume more time than complete sequential techniques. According to the Table 2, GPR–EMI inversions are also faster than EMI–GPR sequential inversions. This is because the calculation times for the first inversion methods dominate the times needed for sequential inversions.

4 CONCLUSIONS

Combining GPR and EMI data for reconstructing multilayered media is promising as the two techniques provide complementary information. Integrated full-waveform EMI and GPR inversion was investigated using numerical experiments to retrieve soil hydrogeophysical properties, comparing different data fusion techniques: weighting methods, Bayesian data fusion and sequential inversion. The joint inversion based on weighting by the inverse of variance is not appropriate for accurate estimation of soil properties from EMI and GPR data. The ideal point approach is more adequate with a better definition of the minimum of the objective functions, though the topography may suffer from flatness in the direction of the parameters which is prejudicial to the accuracy of the parameter estimates. The Bayesian method may represent a good alternative for GPR and EMI data fusion, as it provides accurate estimation of the values with low variance, but it relies on assumptions with regard to the distribution of the parameters. Considering normal distribution as *a priori* information, the Bayesian approach presents more accurate results for our numerical experiments. GPR–EMI inversion approach can accurately estimate the soil electrical parameters when the values of conductivity and permittivity of the first layer are low. For the corresponding configuration, EMI–GPR inversion provides inaccurate estimation of parameter values. The numerical experiments presented in this paper show that the sequential method is highly dependent on the multilayered configuration. The high value of conductivity or permittivity for the first layer reduces the penetration depth of electromagnetic field. As a consequence, sequential inversion scheme is not able to properly estimate electrical properties of the second layer. Partial sequential inversion can improve the results but in some cases it still shows some deviations from the theoretical values.

ACKNOWLEDGMENTS

This research was supported by the Forschungszentrum Jülich (Germany), Université catholique de Louvain and FNRS (Belgium) in the framework of the DIGISOIL project, financed by the European Commission under the 7th Framework Programme for Research and Technological Development, Area 'Environment', Activity 6.3 'Environmental Technologies'.

REFERENCES

al Hagrey, S.A. & Muller, C., 2000. GPR study of pore water content and salinity in sand, *Geophys. Prospect.,* **48**(1), 63–85.

Amezketa, E., 2006. An integrated methodology for assessing soil salinization, a pre-condition for land desertification, *J. Arid Environ.,* **67**(4), 594–606.

Aster, R., Borchers, B. & Thurber, C., 2005. *Parameter Estimation and Inverse Problems* (*International Geophysics*), Elsevier Academic Press, Burlington, MA, 320pp.

Binley, A., Cassiani, G., Middleton, R. & Winship, P., 2002. Vadose zone flow model parameterisation using cross-borehole radar and resistivity imaging, *J. Hydrol.,* **267**(3-4), 147–159.

Bogaert, P. & Fasbender, D., 2007. Bayesian data fusion in a spatial prediction context: a general formulation, *Stochast. Environ. Res. Risk Assess.,* **21**(6), 695–709.

Cameron, D.R., Dejong, E., Read, D.W.L. & Oosterveld, M., 1981. Mapping salinity using resistivity and electromagnetic inductive techniques, *Can. J. Soil Sci.,* **61**(1), 67–78.

Carrera, J. & Neuman, S.P., 1986. Estimation of aquifer parameters under transient and steady state conditions: 1. Maximum likelihood method incorporating prior information, *Water Resour. Res.,* **22**(2), 199–210.

Charnes, A. & Cooper, W. W., 1960. *Management Models and Industrial Applications of Linear Programming*, John Wiley and Sons, New York.

Chen, J.S. & Rubin, Y.R., 2003. An effective Bayesian model for lithofacies estimation using geophysical data, *Water Resour. Res.,* **39**(5), 11.

Chen, J.S., Hubbard, S. & Rubin, Y., 2001. Estimating the hydraulic conductivity at the south oyster site from geophysical tomographic data using Bayesian techniques based on the normal linear regression model, *Water Resour. Res.,* **37**(6), 1603–1613.

Deb, K., Pratap, A., Agarwal, S. & Meyarivan, T., 2002. A fast and elitist multiobjective genetic algorithm: Nsga—II, *IEEE Trans. Evol. Comput.,* **6**(2), 182–197.

Dunn, B.W. & Beecher, H.G., 2007. Using electro-magnetic induction technology to identify sampling sites for soil acidity assessment and to determine spatial variability of soil acidity in rice fields, *Aust. J. Exp. Agric.,* **47**(2), 208–214.

Everett, M.E., Pierce, C.J., Save, N., Warden, R.R., Dickson, D.B., Burt, R.A. & Bradford, J.C., 2006. Geophysical investigation of the June 6, 1944 D-Day invasion site at Pointe Du Hoc, Normandy, France, *Near Surf. Geophys.,* **4**(5), 289–304.

Ezzedine, S., Rubin, Y. & Chen, J.S., 1999. Bayesian method for hydrogeological site characterization using borehole and geophysical survey data: theory and application to the Lawrence Livermore National Laboratory Superfund Site, *Water Resour. Res.,* **35**(9), 2671–2683.

Ferrero, A., Sanpietro, F. & Pisani, U., 1994. Multiport vector network analyzer calibration—a general formulation, *IEEE Trans. Microwave Theory Techniq.,* **42**(12), 2455–2461.

Ghose, R. & Slob, E.C., 2006. Quantitative integration of seismic and GPR reflections to derive unique estimates for water saturation and porosity in subsoil, *Geophys. Res. Lett.,* **33**(5), L05404, doi:10.1029/2005GL025376.

Grandjean, G., Paillou, P., Baghdadi, N., Heggy, E., August, T. & Lasne, Y., 2006. Surface and subsurface structural mapping using low frequency radar: a synthesis of the Mauritanian and Egyptian experiments, *J. Afric. Earth Sci.,* **44**(2), 220–228.

Hedley, C.B., Yule, I.Y., Eastwood, C.R., Shepherd, T.G. & Arnold, G., 2004. Rapid identification of soil textural and management zones using electromagnetic induction sensing of soils, *Aust. J. Soil Res.,* **42**(4), 389–400.

Hendrickx, J.M.H., Baerends, B., Raza, Z.I., Sadig, M. & Chaudhry, M.A., 1992. Soil-salinity assessment by electromagnetic induction of irrigated land, *Soil Sci. Soc. Am. J.,* **56**(6), 1933–1941.

Hiebel, M., 2007. *Fundamentals of Vector Network Analysis*, Rohde and Schwarz, Munich.

Hoekstra, P., Lahti, R., Hild, J., Bates, C.R. & Phillips, D., 1992. Case-histories of shallow time domain electromagnetics in environmental site assessment, *Ground Water Monitor. Remediat.,* **12**(4), 110–117.

Huang, H.P. & Won, I.J., 2003. Characterization of UXO-like targets using broadband electromagnetic induction sensors, *IEEE Trans. Geosci. Remote Sens.,* **41**(3), 652–663.

Huisman, J.A., Hubbard, S.S., Redman, J.D. & Annan, A.P., 2003. Measuring soil water content with ground penetrating radar: a review, *Vadose Zone J.,* **2,** 476–491.

Huyer, W. & Neumaier, A., 1999. Global optimization by multilevel coordinate search, *J. Global Opt.,* **14**(4), 331–355.

Kachanoski, R.G., Gregorich, E.G. & Vanwesenbeeck, I.J., 1988. Estimating spatial variations of soil-water content using noncontacting electromagnetic inductive methods, *Can. J. Soil Sci.,* **68**(4), 715–722.

Kool, J.B. & Parker, J.C., 1988. Analysis of the inverse problem for transient unsaturated flow, *Water Resour. Res.,* **24**(6), 817–830.

Kowalsky, M.B., Finsterle, S., Peterson, J., Hubbard, S., Rubin, Y., Majer, E., Ward, A. & Gee, G., 2005. Estimation of field-scale soil hydraulic and dielectric parameters through joint inversion of GPR and hydrological data, *Water Resour. Res.,* **41,** W11425, doi:10.1029/2005WR004237.

Kozlovskaya, E., Vecsey, L., Plomerova, J. & Raita, T., 2007. Joint inversion of multiple data types with the use of multiobjective optimization: problem formulation and application to the seismic anisotropy investigations, *Geophys. J. Int.,* **171**(2), 761–779.

Ladwig, K.J., 1983. Electromagnetic induction methods for monitoring acid-mine drainage, *Ground Water Monitor. Remediat.,* **3**(1), 46–51.

Lagarias, J.C., Reeds, J.A., Wright, M.H. & Wright, P.E., 1998. Convergence properties of the Nelder-mead simplex method in low dimensions, *SIAM J. Opt.,* **9**(1), 112–147.

Lambot, S., Javaux, M., Hupet, F. & Vanclooster, M., 2002. A global multilevel coordinate search procedure for estimating the unsaturated soil hydraulic properties, *Water Resour. Res.,* **38**(11), 1224, doi:10.1029/2001WR001224.

Lambot, S., Slob, E.C., van den Bosch, I., Stockbroeckx, B. & Vanclooster, M., 2004. Modeling of ground-penetrating radar for accurate characterization of subsurface electric properties, *IEEE Trans. Geosci. Remote Sens.,* **42,** 2555–2568.

Lambot, S., Slob, E. & Vereecken, H., 2007. Fast evaluation of zero-offset Green's function for layered media with application to ground-penetrating radar, *Geophys. Res. Lett.,* **34**(21), doi:10.1029/2007GL031459.

Lesch, S.M., Herrero, J. & Rhoades, J.D., 1998. Monitoring for temporal changes in soil salinity using electromagnetic induction techniques, *Soil Sci. Soc. Am. J.,* **62,** 232–242.

Lines, L.R., Schultz, A.K. & Treitel, S., 1988. Cooperative inversion of geophysical-data, *Geophysics,* **53**(1), 8–20.

Martens, J., Judge, D. & Bigelow, J., 2005. Multiport vector network analyzer measurements, *IEEE Microwave Mag.,* **6**(4), 72–81.

McBratney, A.B., Minasny, B. & Whelan, B.M., 2005. *Obtaining 'Useful' High-resolution Soil Data from Proximally-Sensed Electrical Conductivity/Resistivity (PSEC/R) Surveys*, Precision Agriculture 05, Wageningen Academic Publishers, Wageningen.

Moghadas, D., Andre, F., Vereecken, H. & Lambot, S., 2010. Efficient loop antenna modeling for zero-offset, off-ground electromagnetic induction in multilayered media, *Geophys.,* in press.

Moorkamp, M., Jones, A.G. & Eaton, D.W., 2007. Joint inversion of teleseismic receiver functions and magnetotelluric data using a genetic algorithm: are seismic velocities and electrical conductivities compatible? *Geophys. Res. Lett.,* **34**(16), doi:10.1029/2007GL030519.

Nakashima, Y., Zhou, H. & Sato, M., 2001. Estimation of groundwater level by GPR in an area with multiple ambiguous reflections, *J. appl. Geophys.,* **47,** 241–249.

Pasion, L.R., Billings, S.D., Oldenburg, D.W. & Walker, S.E., 2007. Application of a library based method to time domain electromagnetic data for the identification of unexploded ordnance, *J. appl. Geophys.,* **61**(3–4), 279–291.

Petersen, H., Fleige, H., Rabbel, W. & Horn, R., 2005. Applicability of geophysical prospecting methods for mapping of soil compaction and variability of soil texture on farm land, *J. Plant Nutrit. Soil Sci.–Zeitschrift Fur Pflanzenernahrung Und Bodenkunde,* **168**(1), 68–79.

Reedy, R.C. & Scanlon, B.R., 2003. Soil water content monitoring using electromagnetic induction, *J. Geotech. Geoenviron. Eng.,* **129**(11), 1028–1039.

Sherlock, M.D. & McDonnell, J.J., 2003. A new tool for hillslope hydrologists: spatially distributed groundwater level and soilwater content measured using electromagnetic induction, *Hydrol. Process.,* **17**(10), 1965–1977.

Simunek, J., Sejna, M. & van Genuchten, M.T., 1998. The HYDRUS-1D software package for simulating water flow and solute transport in two-dimensional variably saturated media, Version 1.0. IGWMC-TPS 70, International Ground Water Modeling Center, Colorado School of Mines, Golden, CO.

Srinivas, N. & Deb, K., 1994. Multiobjective optimization using non-dominated sorting in genetic algorithms, *J.Evol. Comput.,* **2**(3), 221–248.

Triantafilis, J. & Lesch, S.M., 2005. Mapping clay content variation using electromagnetic induction techniques, *Comput. Electron. Agric.,* **46**(1–3), 203–237.

Vrugt, J.A. & Robinson, B.A., 2007. Improved evolutionary optimization from genetically adaptive multimethod search, *Proc. Natl. Acad. Sci. U.S.A.,* **104**(3), 708–711.

Vrugt, J.A., van Belle, J. & Bouten, W., 2007. Pareto front analysis of flight time and energy use in long-distance bird migration, *J. Avian Biol.,* **38**(4), 432–442.

Zeleny, M., 1982. *Multiple Criteria Decision Making*, McGraw-Hill, New York.